# CONSEQUENCES OF ENERGY EFFICIENCY MEASURES IMPLEMENTATION TO BUILDINGS' ELECTRICAL SYSTEMS

*Dubravko Franković, Branimir Pavković, Matko Bupić*

Different consequences of energy efficiency measures implementation, in low voltage installations, have been presented and analyzed. Especially, impact of energy inefficient light sources replacement by efficient lamps, and addition of variables speed drives to existing induction machines have been examined. The mentioned impacts have been analyzed on a small low voltage radial distribution network by harmonic power flow calculations. Nonlinear loads were modeled upon laboratory measurements of different compact fluorescent lamps and variable speed drives and harmonic analysis of respective current-voltage waveforms. In addition, impact of variable speed control on refrigeration machines and pumps has been examined and the results presented.

*Keywords: consequences, energy efficiency measures, harmonic load flow, pumps, refrigeration machines*

### Posljedice implementacije mjera energetske učinkovitosti na električne sustave zgrada

U radu su obrađene neke od posljedica inherentnih sustavnom provođenju mjera za povećanje energetske učinkovitosti u niskonaponskim instalacijama zgrada. Posebno je analiziran utjecaj zamjene energetski neučinkovitih izvora svjetlosti učinkovitima te prigradnja frekvencijskih pretvarača postojećim elektromotornim pogonima. Spomenuti utjecaji analizirani su na primjeru male, radijalne distribucijske mreže pomoću metode harmoničkih tokova snaga. Nelinearni tereti modelirani su temeljem strujno-naponskih valnih oblika dobivenih laboratorijskim ispitivanjima fluokompaktnih žarulja različitih proizvođača te elektromotornih pogona s frekvencijskim pretvaračima. Također, u radu je prikazan utjecaj regulacije promjenom brzine vrtnje na pogon rashladnih uređaja i pumpi.

*Ključne riječi: harmonički tokovi snaga, mjere energetske učinkovitosti, posljedice, pumpe, rashladni uređaji*

## 1
## Introduction
## Uvod

The knowledge that primary energy global reserves have a finite quantity is for a longer time a well known fact to a larger population. At the same time, the fact that development and progress imply large energy consumption intensity is generally accepted. Afore mentioned leads to a pair of mutually associated problems – security of supply of sufficient energy amounts and additional environmental impact (e.g. $CO_2$, $NO_x$, $SO_x$ emission). Energy efficiency promotion and adoption of renewable energy sources are techniques used in modern society to deal with problems that arose by the start of the first industrial revolution.

In this paper some of the consequences that come out of building's energy efficiency measures implementation will be analyzed. These consequences are mostly inherent and often disregarded in energy efficiency analysis. Measures that will be dealt with later are: incandescent light sources replacement with compact fluorescent lamps CFLs (energy saving lamps), electromagnetic type ballast with electronic type ballast replacement and variable speed drives implementation. Emphasis is given to consequences of electrical systems energy efficiency improvement.

Special attention will be given to harmonic power flows in low voltage installations. Suitable models of network elements and both linear and nonlinear loads will be developed to adequately analyze consequences of energy efficiency measures implementation to buildings' electrical systems.

## 2
## Energetic, economic and environmental effects of lighting improvements
## Energetski, ekonomski i ekološki utjecaji poboljšanja sustava rasvjete

Experience with energy audits and preliminary energy studies described in [1] has shown that above mentioned measures of lighting improvement, suggested for application to 18 public buildings in Zagreb (total floor area $161\ 000\ m^2$) can result in savings varying between 0 and 21 % of previous total electric energy consumption. The percentage of savings was strongly influenced by the state of previously applied electric loads. Total savings were approximately 730 000 kWh of electric energy and total reduction of $CO_2$ emissions was approximately 500 tons. Calculated annual savings were close to 600 000 kn and payback period was between 2 and 25 years, with average value of 9 years. Such a result can encourage investments into modernization and improvement of the efficiency of lighting.

### 2.1
### Replacement of incandescent with compact fluorescent lamps
### Zamjena žarulja sa žarnom niti fluokompaktnim žaruljama

Undoubtedly, one of the simplest and least expensive measures in energy efficiency improvement is replacement of old, inefficient incandescent light sources with new, energy efficient CFLs. If the chosen alternative CFL has all the necessary characteristics (luminous flux, color temperature, RA factor), a considerable positive effect in electric energy consumption decrease is achieved, as well as decrease in power demand, Tab. 1.
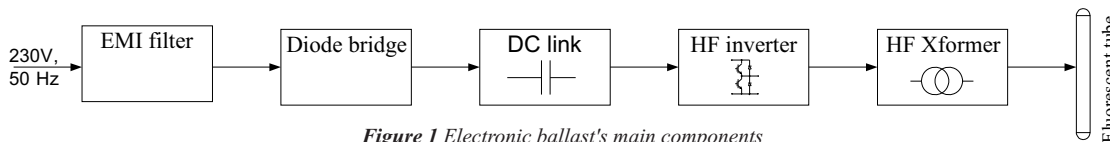
**Figure 1** *Electronic ballast's main components*
**Slika 1.** *Osnovni dijelovi elektroničke prigušnice*

**Table 1** *Characteristic technical parameters of incandescent bulbs and corresponding CFL*
**Tablica 1.** *Karakteristični tehnički parametri žarulja sa žarnom niti i odgovarajućih fluokompaktnih*

| Incandescent lamp power $P_{il}$/W | Corresponding CFL power $P_{fc}$/W | Yearly energy consumption difference, ($t$=2 100 h) $W_y$/kWh | Power demand difference $P_d$/W |
|---|---|---|---|
| 25 | 5 | 42,0 | 20 |
| 40 | 8 | 67,2 | 32 |
| 60 | 12 | 100,8 | 48 |
| 75 | 16 | 123,9 | 59 |
| 100 | 21 | 165,9 | 79 |

The mentioned positive effects are not, though, the only that incur upon CFLs installation. In fact, energy saving CFLs are equipped with electronic ballasts that draw a pulse rather than a sinusoidal current. Since these ballasts are indispensable for their operation, they constitute constantly a highly nonlinear load for the low voltage network thus representing a source of harmonic current. Since the individual power of each energy efficient lamp is rather small, requirements regarding harmonic emissions are not rigorous [2]. Therefore, it is not surprising that some manufacturers produce CFLs with total harmonic distortion (THD) greater than 100 % [3].

Harmonic sources - electronic ballasts, are composed of five essential components: electromagnetic interference filter (EMI), diode type bridge rectifier, DC link – usually a large capacitor, high-frequency inverter whose output signal is in the range of 20-60 kHz and a high-frequency transformer at which the fluorescent tube is connected, Fig. 1.

Extensive laboratory testing has been performed on a number of different CFLs and voltage-current profiles were recorded. Fig. 2, obtained by authors, presents a characteristic current profile for a CFL with respect to applied voltage. The current waveform reveals a highly nonlinear characteristic of the tested energy efficient lamp.
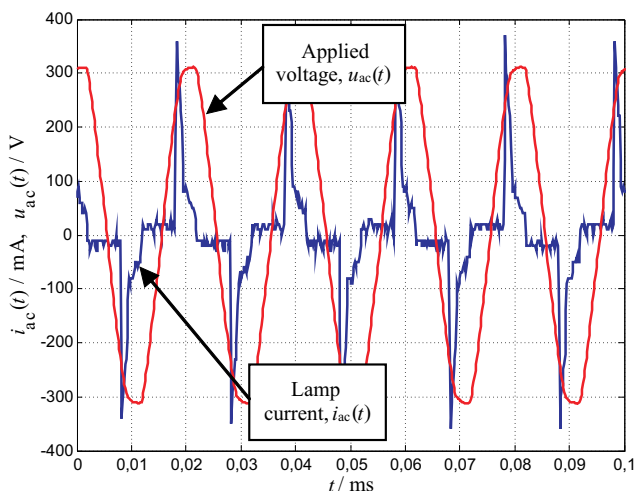


**Figure 2** *CFL's current-voltage profile*
**Slika 2.** *Strujno-naponska karakteristika FK žarulje*

Different authors presented CFL's equivalent models both in time and frequency domain [4, 5].

It is generally agreed that current waveforms, as presented in Fig. 2, can be best described with a differential of two exponential functions and a conductance of constant value $G$, which is determined upon lamp's current RMS value and instantaneous active power [5]:

$$g(t) = G \cdot \left( e^{-\frac{t}{\tau_1}} - e^{-\frac{t}{\tau_2}} \right) \qquad (1)$$

where:
$\tau_1$, $\tau_2$ – are time constants of the two exponential functions, ms
$G$ – denotes the constant value of conductance, S
$t_d$ – is the time delay at start of conducting cycle, ms.

Function $g(t)$ is periodical with time period $T/2$, where $T$ is the fundamental harmonic period. Values of parameters $\tau_1$ and $t_d$ are determined upon measurements of lamp's power factor and THD, for an assumed value of $\tau_2$. Conductance $G$ is determined upon current and active power values.

The other approach is to model CFLs in frequency domain. Such models are usually derived upon the equivalent model presented in Fig. 3.

In [6] nonlinear-load harmonic models were developed by the method of crossed frequency admittance matrix. The term "admittance" is not used as in the classic sense which relates current and voltage of the same frequency. Though, since crossed frequency admittance matrix elements are current to voltage ratios, the term admittance is retained.

By the Fourier analysis of current $i_{ac}(t)$, drawn from the feeding network, Fig. 3, in accordance with [4, 6], the crossed frequency admittance matrix describing CFLs can be constructed:

$$\begin{bmatrix} \dot{I}_1 \\ \dot{I}_3 \\ \dot{I}_5 \\ \vdots \\ \dot{I}_K \end{bmatrix} = \begin{bmatrix} Y_{1,1}^+ & Y_{1,3}^+ & Y_{1,5}^+ & \cdots & Y_{1,H}^+ \\ Y_{3,1}^+ & Y_{3,3}^+ & Y_{3,5}^+ & \cdots & Y_{3,H}^+ \\ Y_{5,1}^+ & Y_{5,3}^+ & Y_{5,5}^+ & \cdots & Y_{5,H}^+ \\ \vdots & \vdots & \vdots & \cdots & \vdots \\ Y_{K,1}^+ & Y_{K,3}^+ & Y_{K,5}^+ & \cdots & Y_{K,H}^+ \end{bmatrix} \cdot \begin{bmatrix} \dot{V}_1 \\ \dot{V}_3 \\ \dot{V}_5 \\ \vdots \\ \dot{V}_{1H} \end{bmatrix} \cdot \qquad (2)$$

Elements of above matrix equation are: column-vector of CFL's harmonic currents, column-vector of the applied harmonic voltages, and the crossed frequency admittance matrix whose elements, self and mutual harmonic admittances, can be computed according to equations (3) and (4):

$$Y_{k,h}^+ = \frac{\sqrt{1 + (h\omega RC)^2}}{\pi R} (\delta - \alpha) \cdot e^{j \cdot \arctan(h\omega RC)}, \text{ for } h = k \qquad (3)$$
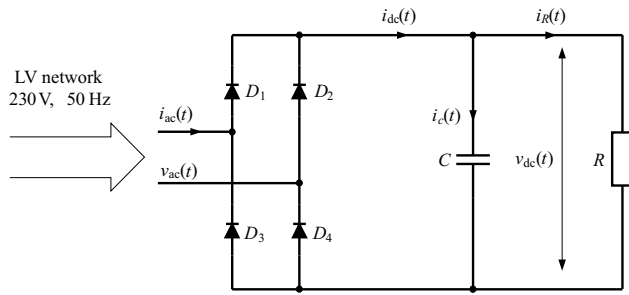
**Figure 3** *CFL model for frequency domain analysis*
**Slika 3.** *Nadomjesni model FK žarulje za analizu u frekvencijskoj domeni*

$$Y_{k,h}^{+} = \frac{2\sqrt{1+(h\omega RC)^2}}{\pi R(h-k)} \cdot \sin\frac{(h-k)(\delta-\alpha)}{2} \cdot$$
$$\cdot e^{j\left(\frac{(h-k)(\delta-\alpha)}{2}+\arctan(h\omega RC)\right)} \quad , \text{for } h \neq k \quad (4)$$

Values of extinction angle $\delta$ and firing angle $\alpha$ are determined upon voltage-current interrelationship of the equivalent circuit presented in Fig. 3. The extinction angle corresponds to the instant when the capacitor's charging current falls to zero, while the firing angle matches the instant when the instantaneous system voltage becomes larger than the capacitor's remaining voltage, which has been discharging through resistance $R$. For capacitance $C$ size, a typical value of 15 μF can be adopted for most standard-type CFLs [4]. The size of resistance $R$ can also be determined in accordance with equations derived in [7] or by the empirical relation [4]:

$$R = \frac{V}{I} , \Omega \quad (5)$$

where $V$ denotes the RMS value of applied voltage, and $I$ denotes the RMS value of the fundamental harmonic component. If such measurements are not readily available, for $V$ a rated value can be adopted and for $I$ a value of 85 % of the declared nominal CFL's current can be used.

## 2.2
## Replacement of electromagnetic with electronic ballasts
Zamjena elektromagnetskih prigušnica elektroničkim

Replacement of electromagnetic ballasts with electronic ballasts is an energy efficiency measure that is conducted in order to achieve energy savings on existing fluorescent lamps. Furthermore, by installment of electronic ballasts, fluorescent lamp's utilization factor is improved, i.e. the lamp draws up to 25 % less power.

Moreover, fluorescent tube's lifetime is prolonged, lamp operation becomes quieter and the lighting reveals a more comfortable characteristic due to the absence of light flickering, inherent to electromagnetic ballasts.

The basic components of electronic ballasts are identical to the ones presented in Fig. 1. Therefore, modeling of electronic ballasts found in modern fluorescent lamps is equal to that presented in chapter 2.1.

Some of the problems and consequences due to ballast replacement are dealt with in [8]. The consequences can be summarized as follows:

- Current THD of a parallel combination of several fluorescent lamps equipped with electromagnetic ballasts remains constant, i.e. it is equal to current THD of only one fluorescent lamp.
- Current THD decreases by parallel connection of fluorescent lamps equipped with electromagnetic and electronic ballasts. Afore-mentioned is a consequence of mutual cancellation of particular harmonic current components, and also due to lower current consumption of electronic ballasts.
- Combination of fluorescent lamps equipped with electromagnetic ballasts with "older generation" electronic ballasts and "new generation" ballasts results in a further decrease of current consumption.
- Neutral conductor current values recorded in 4-wire 3-phase installations were: 48,3 % of the respective phase current value for lighting realized with exclusively electromagnetic ballasts, 90,1 % for "older generation" electronic ballasts and 14,3 % for "newer generation" electronic ballasts. Neutral conductor's current, in absolute value, increased by 13 % in installations with "older generation" electronic ballasts and decreased by 82 % in installations with "newer generation" ballasts as compared to the installation with solely electromagnetic ballasts.
- Voltage THD along the main feeder to which the installation is connected decreases when all the electromagnetic ballasts are replaced by electronic ballasts.

## 3
## Addition of variable speed drives to existing non-controlled induction machines
Prigradnja frekventnih regulatora brzine vrtnje postojećim nereguliranim elektromotornim pogonima

Addition of variable speed drives (VSD) to existing electric machines is also an energy efficiency measure by which a substantial amount of electric energy can be saved. The VSD adjusts, in every instant, machine's speed to instantaneous demand [9].

Energy consumption of compressors in refrigeration equipment used for air-conditioning of buildings is significant. In the explanation that follows, the principles of vapor compression refrigeration system are explained in order to identify the influence of VSD on compressor energy consumption.

The simplest vapor compression refrigeration circuit usually used in air – conditioning applications consists of the evaporator, compressor, condenser and the throttling valve, Fig. 4. Refrigerant evaporates in the evaporator at pressure $p_e$ and corresponding saturation temperature $T_e$. Evaporation heat is supplied by the cooled fluid with mass flow $\dot{M}_{Fe}$ entering temperature $T_{Fe,1}$ and leaving temperature $T_{Fe,2}$. Saturated (or superheated) vapor 1 enters the compressor. Refrigerant leaves compressor with high pressure $p_c$ and temperature $T_2$, which is higher than the saturation temperature $T_c$, Fig. 5. In order to enable condensation, saturation temperature $T_c$ has to be higher than the temperature of the condenser cooling fluid whose mass flow is $\dot{M}_{Fc}$, entering temperature $T_{Fc,1}$ and leaving temperature $T_{Fc,2}$. Liquid refrigerant (saturated or subcooled liquid) leaves condenser and enters throttling valve, where the pressure of the refrigerant is reduced from $p_c$ to $p_e$. Saturation temperature for the pressure $p_e$ is $T_e$, and it is constant for a single – component refrigerant.

Condenser heat $\dot{Q}_c$, which can be approximated as the sum of the cooling load and compressor power is rejected to the surroundings in the condenser:

$$\dot{Q}_c = \dot{Q}_e + \dot{P} \text{, W} \tag{6}$$

Energy efficiency ratio (*EER*) of a refrigeration machine is a quotient between the heat removed from the cooled fluid in the evaporator and the consumed energy for running the compressor:

$$EER = \frac{\dot{Q}_e}{\dot{P}}. \tag{7}$$

In some cases it is expressed as a quotient between the evaporator heat load and the power necessary for running the entire refrigeration machine (compressor as well as fans and other equipment necessary for operation), [10].
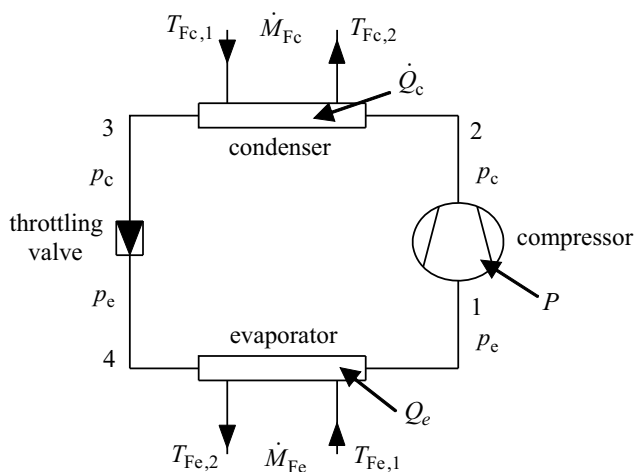
**Figure 4** *Layout of a vapor compression refrigeration system with single stage compression and throttling*
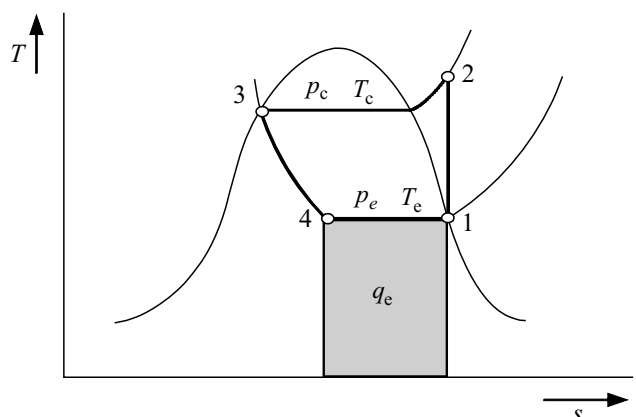**Slika 4.** *Shema parnog kompresijskog rashladnog uređaja s jednostupanjskom kompresijom i prigušenjem*

**Figure 5** *T,s- diagram for a vapor compression refrigeration process with single stage compression and throttling*
**Slika 5.** *T,s- dijagram parnog kompresijskog rashladnog procesa s jednostupanjskom kompresijom i prigušenjem*

An example of $\dot{Q}_e$, $\dot{P}$ and *EER* as a function of temperatures $T_c$ and $T_e$ in the process is presented in Figures 7, 8 and 9. It has been achieved from factory data of a particular water chiller compressor, but it represents general behavior of refrigeration equipment.
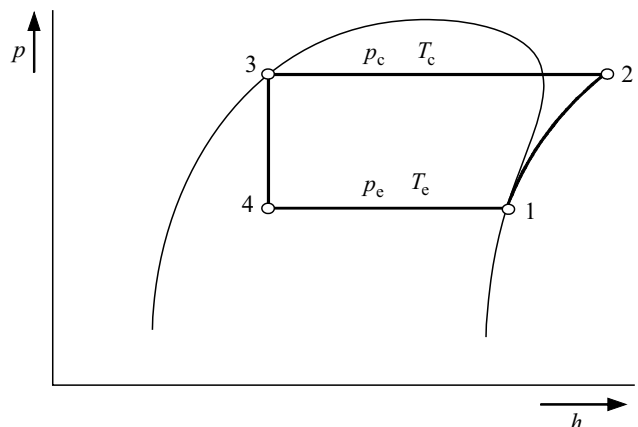
**Figure 6** *p,h- diagram for a vapor compression refrigeration process with single stage compression and throttling*
**Slika 6.** *p,h- djiagram parnog kompresijskog rashladnog procesa s jednostupanjskom kompresijom i prigušenjem*
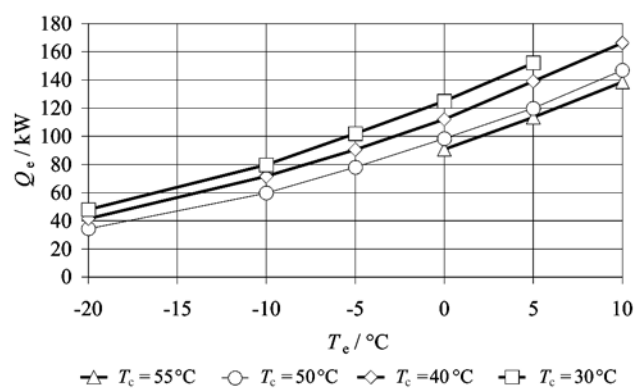
**Figure 7** *Changes of cooling load with condensing and evaporation temperatures*
**Slika 7.** *Promjena rashladnog učinka s promjenom temperature kondenzacije i isparivanja*
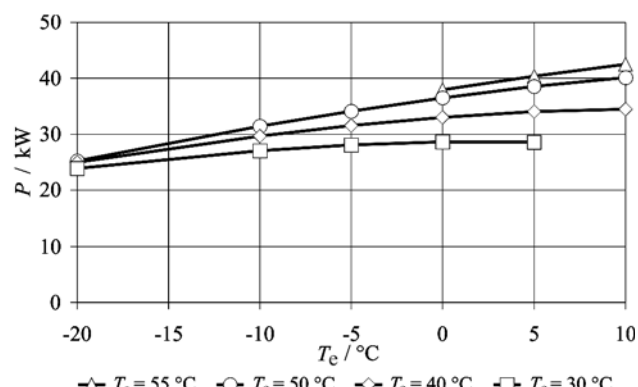
**Figure 8** *Changes of absorbed compressor power with condensing and evaporation temperatures*
**Slika 8.** *Promjena apsorbirane snage kompresora s promjenom temperature kondenzacije i isparivanja*

For the same evaporation temperature $T_e$, decrease of the condensing temperature $T_c$ results in higher value of *EER*. Also, for the same condensing temperature $T_c$, decrease of the evaporating temperature $T_e$ results in lower value of *EER*, Fig. 9.

Evaporator load $\dot{Q}_e$ (kW) depends on refrigerant mass flow rate $\dot{M}_R$ (kg/s) as well as on the difference between specific enthalpies of the refrigerant at evaporator outlet $h_1$ and evaporator inlet $h_4$, Fig. 6:
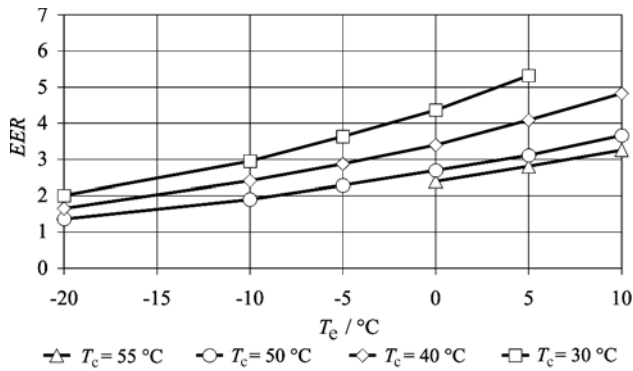
$$\dot{Q}_e = \dot{M}_R \cdot (h_1 - h_4). \tag{8}$$

**Figure 9** *Changes of EER with condensing and evaporation temperatures*
**Slika 9.** *Promjena EER s promjenom temperature kondenzacije i temperature isparivanja*

Those enthalpies vary with evaporation and condensation temperature within the process.

Refrigerant mass flow can be evaluated from refrigerant effective volumetric flow $\dot{V}_{\text{eff}}$ (m³/s) at compressor inlet as:

$$\dot{M} = \dot{V}_{\text{eff}} \cdot \rho_1 . \tag{9}$$

Refrigerant density at compressor inlet $\rho_1$ (kg/m³) is also variable and depends on operating conditions. Theoretical volumetric flow for a compressor with cylinder diameter $d$ (m), piston stroke $s$ (m), number of cylinders $z$ and rotation speed $n$ (1/s) is:

$$\dot{V}_{\text{t}} = V_{\text{s}} \cdot z \cdot n = \frac{d^2 \cdot \pi}{4} \cdot s \cdot z \cdot n . \tag{10}$$

Effective refrigerant volumetric flow is lower than theoretical, and the difference is expressed through the volumetric efficiency $\lambda < 1$:

$$\dot{V}_{\text{eff}} = \lambda \cdot \dot{V}_{\text{t}} . \tag{11}$$

Finally, by introducing (10) and (11) into (9), the compressor mass flow can be expressed as:

$$\dot{M} = \lambda \frac{d^2 \cdot \pi}{4} \cdot s \cdot z \cdot n \cdot \rho_1 \tag{12}$$

and with (8) and (12), the evaporator load of the refrigeration machine is:

$$\dot{Q}_{\text{e}} = \lambda \frac{d^2 \cdot \pi}{4} \cdot s \cdot z \cdot n \cdot \rho_1 \cdot \left( h_1 - h_4 \right). \tag{13}$$

Heat exchanged in a heat exchanger with heat exchange area $A$ (m²), overall heat transfer coefficient $k$ (W/(m²·K)) and mean temperature difference $\Delta T_{\text{m}}$ (K) can be expressed as:

$$\dot{Q} = k \cdot A \cdot \Delta T_{\text{m}} \tag{14}$$

where:

$$\Delta T_{\text{m}} = \frac{\Delta T' - \Delta T''}{\ln \dfrac{\Delta T'}{\Delta T''}} \tag{15}$$

as presented in Fig. 10.

The same heat has to be transported as the sensible heat of the heat transfer fluid whose mass flow is $\dot{M}_{\text{F}}$ (kg/s) and specific thermal capacity $c_{\text{F}}$ (J/(kg·K)):

$$\dot{Q} = \dot{M}_{\text{F}} \cdot c_{\text{F}} \cdot \left( T_1'' - T_1' \right). \tag{16}$$

Inlet temperatures of the cooled fluid in the evaporator and the cooling fluid in the condenser depend on design features and dynamic behavior of heat rejection system and cooling load distribution system. Those temperatures cannot be influenced only by control action of the refrigeration machine controller. When VSD is used, the decrease of the compressor speed $n$ due to the action of the controller decreases the mass flow of the refrigerant (12) decreasing thus evaporator load $\dot{Q}_e$ (13) as well as condenser load and condenser (6). For a constant mass flow of the heat transfer fluid $\dot{M}_{\text{F}}$ in each heat exchanger, temperature differences of heat transfer fluids ($T_1'' - T_1'$) decrease, as well as the mean temperature difference $\Delta T_{\text{m}}$. As fluid inlet temperatures $T_1'$ are not influenced, those remain constant, but outlet temperature $T_1''$ decreases in the condenser and increases in the evaporator. The final consequence of reduced compressor speed is decreased evaporator load $\dot{Q}_{\text{e}}$, decreased condenser load $\dot{Q}_{\text{c}}$, increased evaporation temperature $T_{\text{e}}$ and decreased condensing temperature $T_{\text{c}}$, Fig. 11. For those new operation conditions *EER* increases, Fig. 9, which means that the refrigeration circuit operates more efficiently.

Such a system behaviour is important, because all cooling systems operate most of their operation time in partial cooling loads. When chillers for building cooling are considered, the European Seasonal Energy Efficiency Ratio (ESEER) is used. It is a weighed formula enabling to take
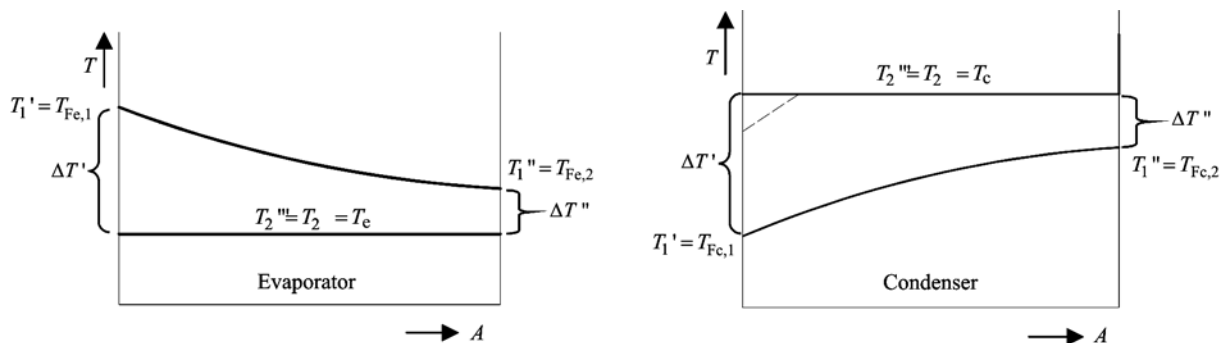


**Figure 10** *Temperatures in the evaporator and condenser of a refrigeration machine*
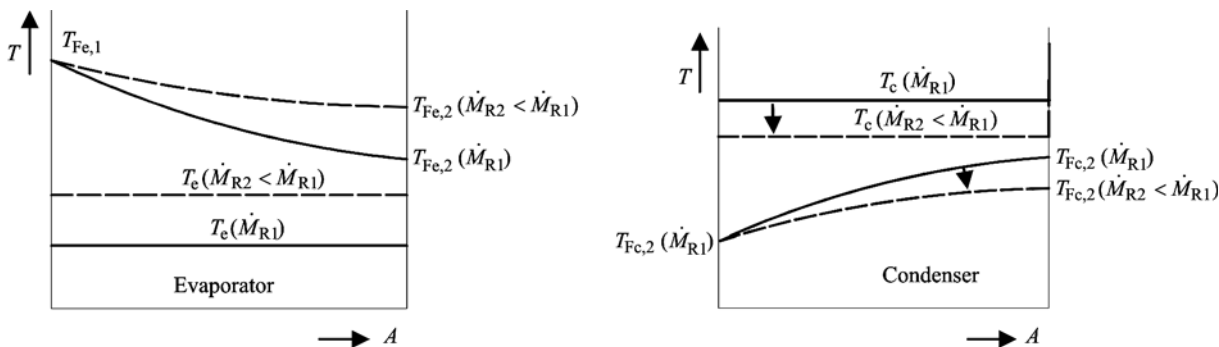**Slika 10.** *Temperatura u isparivaču i kondenzatoru rashladnog uređaja*

***Figure 11*** *Influence of the reduction of refrigerant mass flow on temperatures in the evaporator and condenser of a refrigeration machine*
***Slika 11.*** *Utjecaj smanjivanja masenog protoka radne tvari na temperature u isparivaču i kondenzatoru rashladnog uređaja*

into account the variation of *EER* with the load rate of buildings and the variation of air or water inlet condenser temperature [10]. *ESEER* is calculated as follows:

$$ESEER = A \cdot EER_{100\,\%} + B \cdot EER_{75\,\%} + C \cdot EER_{50\,\%} + \\ + D \cdot EER_{25\,\%}. \tag{17}$$

Assumed weighting coefficients $A = 0{,}03$; $B = 0{,}33$; $C = 0{,}41$; $D = 0{,}23$ mean that 3 % of delivered cooling energy is removed from the building at full load, 33 % at 75 % of full load, 41 % at 50 % of full load and 23 % at 25 % of full load. *ESEER* is a realistic tool, much better than full load *EER*, to be used to compare average efficiency of two chillers. However it must be kept in mind that *ESEER* cannot be used to calculate exact energy consumption for a particular use in a particular geographic position [10].

When VSD is provided, significant energy savings can be achieved compared to systems operating without such a refrigerant flow control.

New generations of refrigeration compressors, especially those used for air – conditioning applications are usually equipped with VSDs. When retrofit of the refrigeration machines is planned as a part of energy efficiency measures, addition of VSD to existing refrigeration compressor should be carefully considered

from the viewpoint of technical conditions for implementation, but also from the viewpoint of economic feasibility for each particular case [11].

VSDs are especially suitable to drive centrifugal pumps and fans whose power rises with the cube of rotational speed (e.g. a centrifugal drive operating at 50 % of rated speed draws 12,5 % of its rated power from the feeding network if VSD losses are neglected).

Operation with partial loads is also common for heating systems, as heating load decreases with decreasing external air temperatures.

Supply water temperature to heat exchangers in heated spaces can be decreased accordingly and control system maintains supply temperature or heat transfer flow through the exchange on desired level.

Throttling the heat transfer fluid flow without VSD of a pump (case a, Fig. 12) does not decrease pump energy consumption and causes problems with noise and the precise control in the heating system. Application of three way valves (case b, Fig. 12) solves the problem with noise and proper control, but pump energy consumption remains the same. Application of VSD for a pump, with provided maintaining of constant static pressure difference in the water loop (case c, Fig. 12), leads to a simple and efficient control with significantly decreased energy consumption of the pump. Similar considerations are valuable for air
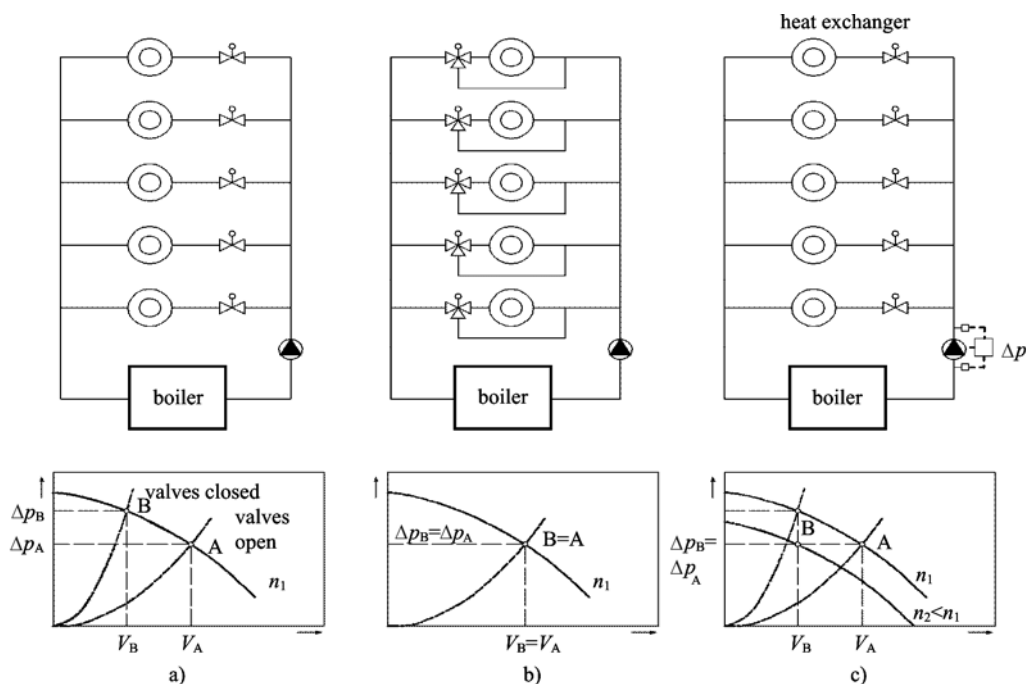


***Figure 12*** *Control of heating systems*
***Slika 12.*** *Regulacija u sustavima grijanja*

systems with centrifugal fans.

Furthermore, VSDs allow synchronization of rotational speed with production process needs, steadier machine operation, specifically machine soft-starting and soft-arresting. VSDs necessitate minimal maintenance, whilst prolonging plant's life-time.

Surveying studies presented in [1], it can be observed that VSDs were not suggested as an energy efficiency measure in any of those studies. The main reason was the necessary level of analysis. In fact, all conducted studies were contracted at a level of preliminary energy study, while the implementation of VSDs demands a different, more complex approach that corresponds to a detailed energy study, which means higher resources that had not been contracted.

The majority of VSDs intended to be used in electric motor drives have at their input a bridge rectifier. At their output an inverter converts DC voltage to AC voltage of variable amplitude and frequency, thus providing variable speed to induction machine.

A diode bridge rectifier is most frequently used as an AC voltage rectifier. An appropriate capacitor is connected to the DC bus to provide additional smoothing of the rectified voltage, Fig. 13.
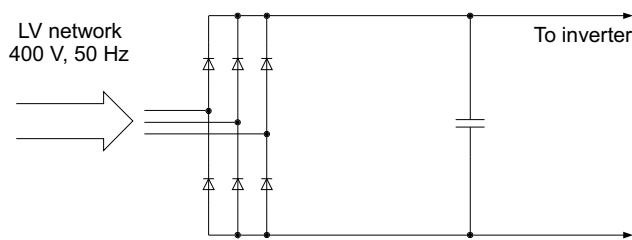


**Figure 13** *VSD's three-phase bridge rectifier for PWM drives*
**Slika 13.** *Trofazni ispravljač u mosnom spoju PWM frekvencijskog pretvarača*

The current that such rectifier circuit draws from the feeding network is non-sinusoidal and consists of two separate pulses per half-period. As a consequence large current distortion incurs, and the electric motor drive itself appears as a nonlinear load, Fig. 14.
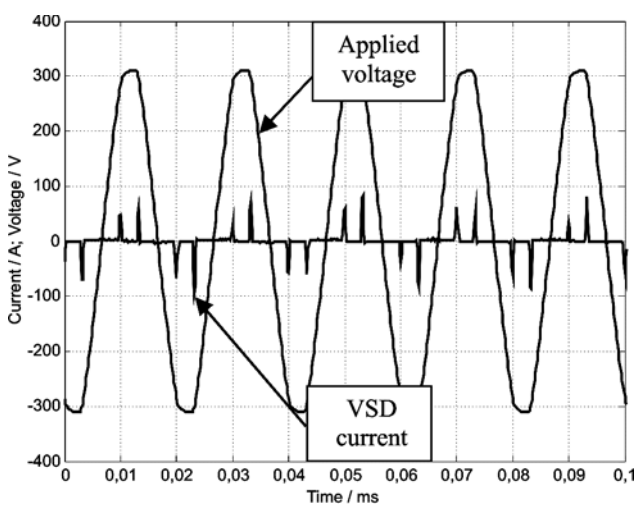


**Figure 14** *Voltage-current waveforms for a VSD controlled induction machine*
**Slika 14.** *Strujno-naponski valni oblici na ulazu frekvencijskog pretvarača elektromotornog pogona*

Frequency coupling matrices representing VSDs harmonic models, similar to the one presented for CFLs, can be found in [12, 13].

Characteristic current harmonics, which are therefore generated, depend on the number of rectifiers (pulse number) used in a circuit, and can be determined from the following equation:

$$h = (n \cdot p) \pm 1, \ n = 1, 2, 3, 4, 5,... , \tag{18}$$

where $p$ denotes the number of rectifier pulsations.

Therefore, for the bridge rectifier presented in Fig. 13, harmonics of order 5., 7., 11., 13., 17., 23., 25., … can be expected. The characteristic harmonic number and its amplitude primarily depend on rectifier technology and non-linear load with feeding network impedance mutual interrelationship. In fact, impedance size between the rectifier and electric energy source – feeding network, determines harmonics amplitude and therefore harmonic voltages throughout the distribution network, Fig. 15.
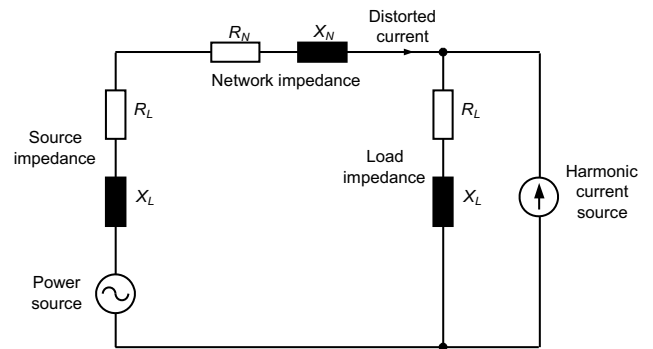


**Figure 15** *Non-linear load impact on distribution network*
**Slika 15.** *Utjecaj nelinearnog tereta na distribucijsku mrežu*

The distorted current flow through distribution network impedances causes a voltage drop or harmonic voltage distortion. This relationship is proportional to the level of distribution system available fault current and to distribution system design. If available fault current is high (stiff system) the distribution system impedance is low as is low harmonic distortion. A low available fault current (weak system) corresponds to high distribution network impedance and high harmonic distortion.

Negative consequences of VSD operation can be summarized as follows [14]:
- Conductor overheating since conductor heating is a function of the square RMS current per unit volume of the conductor. Harmonic currents on undersized conductors or cables can cause "skin effect", which increases with frequency.
- Capacitor overheating and reduced life-time can be affected due to increased power losses. If capacitors are tuned to one of the characteristic harmonics such as 5th or 7th, overvoltage and resonance can cause dielectric breakdown and failure.
- Harmonics can cause breaker and fuse false or spurious operations and trips, damaging or blowing components for no apparent reason, causing discontinuities in LV customer supply.
- Increased iron and copper losses in transformers due to stray flux losses. This causes excessive overheating of transformer windings.
- Generators are subject to similar problems as

transformers. Sizing and coordination is critical to operation of voltage regulators and controls. Excessive harmonic voltage distortion can cause multiple zero crossing of the current waveform, which affects voltage regulator timing and causes interference and instability.

- Utility meters may incorrectly record measurements, resulting in higher billings to customers.
- Power supplies and VSDs can be affected by misoperation due to current multiple zero crossing. Harmonics can cause failure of commutation circuits, found in DC drives and AC drives.
- Computers and telephone lines may experience interference and failures.

# 4
## Radial distribution network harmonic power flow
### Harmonički tokovi snaga u radijalnoj distribucijskoj mreži

Low voltage network power flow is usually performed during design stages of LV electric installation projects and development studies. Such calculations are rather simple and readily give results sufficient for equipment dimensioning and selection. However, these calculations rarely encompass all the peculiarities and effects that nonlinear loads, such as CFLs, VSDs and PCs, manifest on phase voltages and currents.

Besides, these calculations do not give insight into voltage-current profiles on all physically existing conductors – phase conductors, neutral conductor and protective earth conductor.

In order to get insight into consequences of building's energy efficiency measures implementation in electric systems a calculation methodology, based on harmonic power flow and [15-17], is developed. Fig. 16 shows main parts of the proposed algorithm.
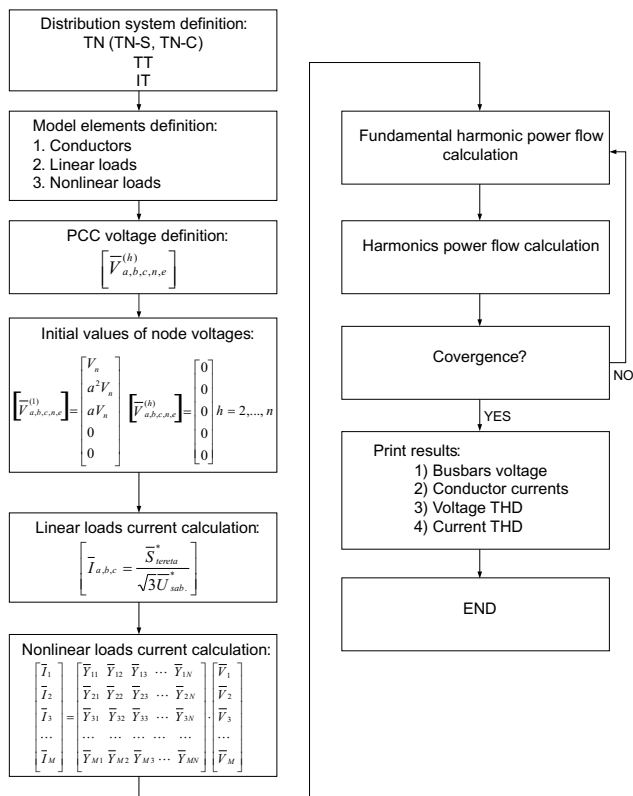


**Figure 16** *Block diagram of LV installation harmonic power flow*
**Slika 16.** *Blok djiagram harmoničkih tokova snaga u niskonaponskoj instalaciji*

The algorithm starts by LV network distribution type definition, since this determines important voltage-current relationships, Fig. 17.
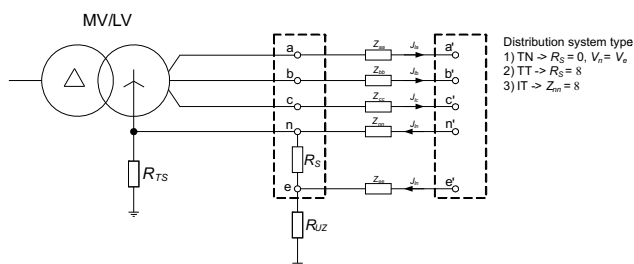


**Figure 17** *Distribution system type impact on voltage-current relationships*
**Slika 17.** *Utjecaj tipa razvodnog sustava na strujno-naponske odnose*

Distribution network harmonic power flow is commonly performed in two successive steps, repeated iteratively, until convergence:
1) Backward current sweep and
2) Forward voltage sweep.

On a simple LV installation, presented in Fig. 18, the proposed methodology will be demonstrated and results compared to results obtained with classic non-harmonic voltage drop calculation. Also, obtained results give insight into building's energy efficiency measures implementation consequences.

Low voltage network node numeration starts with node 1 – the feeding point, and increases with the downstream distance. The more distant a node is from the feeding point the higher its node number.

## 4.1
### Backward current sweep
#### Postupak s desna na lijevo za struje

Backward current sweep consists of load current summation starting from the node that has the highest node number and moving towards the feeding point - node 1. Equation (19) is separately solved for the fundamental harmonic and separately for all other harmonics of interest. The $[J_l]^{(h),k}$ vector-column represents the power flow on the $l$-th network branch, and vector-columns $[I_l]^{(h),k}$ and $[J_m]^{(h),k}$ represent current injection at node $j$ and all current injections downstream of node $j$:

$$\begin{bmatrix} \bar{J}_{la} \\ \bar{J}_{lb} \\ \bar{J}_{lc} \\ \bar{J}_{ln} \\ \bar{J}_{le} \end{bmatrix}^{(h),k} = - \begin{bmatrix} \bar{I}_{ja} \\ \bar{I}_{jb} \\ \bar{I}_{jc} \\ \bar{I}_{jn} \\ \bar{I}_{je} \end{bmatrix}^{(h),k} + \sum_{m \in \Omega_j} \begin{bmatrix} \bar{J}_{ma} \\ \bar{J}_{mb} \\ \bar{J}_{mc} \\ \bar{J}_{mn} \\ \bar{J}_{me} \end{bmatrix}^{(h),k}. \tag{19}$$

## 4.2
### Forward voltage sweep
#### Postupak s lijeva na desno za napone

Adversely to backward current sweep, the forward sweep starts at node 1 and goes towards downstream

nodes. Voltage at node 1 is supposed to be nominal. However, it is possible to calculate assuming a different value than rated voltage at node 1. In all following calculations, rated voltage at node 1 is assumed throughout the iterative process. Furthermore, in the first iteration rated voltage of all network nodes is assumed. The potential of neutral conductor and protective earth conductor throughout the installation is assumed to be zero. Similarly, initial values of voltage harmonics at all LV network nodes are assumed to be zero. Equation (20) is solved separately for the fundamental harmonic and separately for all other harmonics of interest.

The voltage drop between nodes $i$ and $j$ for the $h$-th harmonic in $k$-th iteration is:

$$
\begin{bmatrix} \bar{V}_{ia} \\ \bar{V}_{ib} \\ \bar{V}_{ic} \\ \bar{V}_{in} \\ \bar{V}_{ie} \end{bmatrix}^{(h),k} - \begin{bmatrix} \bar{V}_{ja} \\ \bar{V}_{jb} \\ \bar{V}_{jc} \\ \bar{V}_{jn} \\ \bar{V}_{je} \end{bmatrix}^{(h),k} = \begin{bmatrix} \bar{Z}_{aa} & \bar{Z}_{ab} & \bar{Z}_{ac} & \bar{Z}_{an} & \bar{Z}_{ae} \\ \bar{Z}_{ba} & \bar{Z}_{bb} & \bar{Z}_{bc} & \bar{Z}_{bn} & \bar{Z}_{be} \\ \bar{Z}_{ca} & \bar{Z}_{cb} & \bar{Z}_{cc} & \bar{Z}_{cn} & \bar{Z}_{ce} \\ \bar{Z}_{na} & \bar{Z}_{nb} & \bar{Z}_{nc} & \bar{Z}_{nn} & \bar{Z}_{ne} \\ \bar{Z}_{ea} & \bar{Z}_{eb} & \bar{Z}_{ec} & \bar{Z}_{en} & \bar{Z}_{ee} \end{bmatrix}^{(h)} \cdot
$$

$$
\cdot \begin{bmatrix} \bar{J}_{la} \\ \bar{J}_{lb} \\ \bar{J}_{lc} \\ \bar{J}_{ln} \\ \bar{J}_{le} \end{bmatrix}^{(h),k} . \tag{20}
$$

Impedance matrix $[Z]^{(h)}$ is determined separately for each harmonic. The matrix is symmetrical and has as many rows and columns as there are conductors that physically connect nodes $i$ and $j$. If potentials of neutral and protective earth conductors are not of special interest, corresponding rows and columns in the impedance matrix can be eliminated, and further calculation is performed on a matrix of size 3×3.

## 4.3
## Low voltage cables modeling
Modeliranje niskonaponskih kabela

Low voltage conductors and cables are modeled in accordance to [18, 19]. Low voltage cable capacitance is neglected due to its small value. Therefore, cable and conductor equivalent model consists of 3, 4 or 5 mutually coupled impedances, depending on the number of physically present wires. Respective relations for 3, 4 and 5 wire cables are derived and the results presented in Tab. 2.

Applying relations presented in Tab. 2 and cable technical data conductor impedance matrices are calculated for all LV network branches. The conductor impedance matrix describing e.g. the cable denoted *B1*, Fig. 18, with conductors in flat formation, at fundamental frequency, is as follows:

## 4.4
## Low voltage load modeling
Modeliranje niskonaponskih tereta

Adequate load modeling is essential to correctly perform the radial distribution harmonic power flow. Load modeling by crossed frequency admittance matrix has proven to be an advantageous method to precisely describe both linear and non-linear loads.

In accordance with [4], currents and voltages of a load are related by matrix equation (21).

$$
\begin{bmatrix} \bar{I}_1 \\ \bar{I}_2 \\ \bar{I}_3 \\ \vdots \\ \bar{I}_M \end{bmatrix} = \begin{bmatrix} Y_{1,1} & Y_{1,2} & Y_{1,3} & \cdots & Y_{1,N} \\ Y_{2,1} & Y_{2,2} & Y_{2,3} & \cdots & Y_{2,N} \\ Y_{3,1} & Y_{3,2} & Y_{3,3} & \cdots & Y_{3,N} \\ \vdots & \vdots & \vdots & \cdots & \vdots \\ Y_{M,1} & Y_{M,2} & Y_{M,3} & \cdots & Y_{M,N} \end{bmatrix} \cdot \begin{bmatrix} \bar{V}_1 \\ \bar{V}_2 \\ \bar{V}_3 \\ \vdots \\ \bar{V}_N \end{bmatrix} . \tag{21}
$$

If a load is linear, then the crossed frequency matrix becomes diagonal. For nonlinear loads the matrix isn't diagonal, and matrix elements need not be constant, but are rather voltage dependent. The procedure of computing matrix elements consists of two steps:
1) To a nonlinear load fundamental frequency voltage is applied and the phase currents are measured, thus enabling one to calculate the following matrix elements:

$$
\bar{Y}_{k,1} = \frac{\bar{I}_k}{\bar{V}_1}, k = 1, 2, ..., M . \tag{22}
$$

2) In addition to the fundamental frequency voltage, successively, one by one, harmonic voltage components are applied to the nonlinear load and again phase harmonic currents are measured allowing to calculate all the other matrix elements:
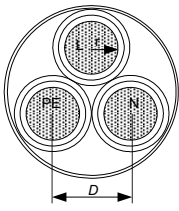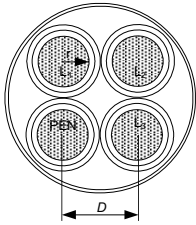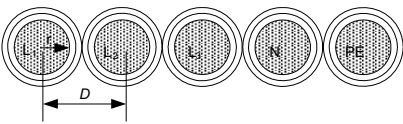
$$
\bar{Y}_{k,j} = \frac{\bar{I}_k - \bar{Y}_{k,1} \cdot \bar{V}_1}{\bar{V}_j}, k = 1, 2, ..., M; \; j \neq 1 . \tag{23}
$$

A different approach is to calculate, both linear and nonlinear load's injected currents, knowing apparent power, power factor and bus voltage.

For non-linear loads Norton's harmonic equivalents can be calculated upon equipment's declared technical data or, again, by measurements.

Hereafter for a radial distribution network, shown in Fig. 18, harmonic power flow calculation results are presented. Nonlinear load models have been determined using results from laboratory measurements.

$$
\left[\bar{Z}^{\text{conductor}}\right] = \begin{bmatrix} 0{,}0616 + j0{,}0172 & 0 + j0{,}0146 & 0 + j0{,}0137 & 0 + j0{,}0132 & 0 + j0{,}0128 \\ 0 + j0{,}0146 & 0{,}0616 + j0{,}0172 & 0 + j0{,}0146 & 0 + j0{,}0137 & 0 + j0{,}0132 \\ 0 + j0{,}0137 & 0 + j0{,}0146 & 0{,}0616 + j0{,}0172 & 0 + j0{,}0146 & 0 + j0{,}0137 \\ 0 + j0{,}0132 & 0 + j0{,}0137 & 0 + j0{,}0146 & 0{,}0616 + j0{,}0172 & 0 + j0{,}0146 \\ 0 + j0{,}0128 & 0 + j0{,}0132 & 0 + j0{,}0137 & 0 + j0{,}0146 & 0{,}0616 + j0{,}0172 \end{bmatrix}, \Omega .
$$

**Table 2** *Low voltage cable impedance matrices for radial distribution harmonic load flow analysis*
**Tablica 2.** *Matrice impedancija niskonaponskih kabela za proračun harmoničkih tokova snaga u radijalnim distribucijskim mrežama*

| Conductor configuration | Conductor impedance matrix | Impedance values $Z\,/\,\Omega/\text{km}$ |
|---|---|---|
| | $$\begin{bmatrix} \overline{Z}_{L,L} & \overline{Z}_{L,N} & \overline{Z}_{L,PE} \\ \overline{Z}_{L,N} & \overline{Z}_{N,N} & \overline{Z}_{N,PE} \\ \overline{Z}_{L,PE} & \overline{Z}_{N,PE} & \overline{Z}_{PE,PE} \end{bmatrix}$$ | $\overline{Z}_{L,L} = \overline{Z}_{N,N} = \overline{Z}_{PE,PE} =$ $r_v + j0{,}0628\!\left(\ln\dfrac{1}{r'} + 6{,}836\right)$ $\overline{Z}_{L,N} = \overline{Z}_{L,PE} = \overline{Z}_{N,PE} =$ $j0{,}0628\!\left(\ln\dfrac{1}{D} + 6{,}836\right)$ |
| | $$\begin{bmatrix} \overline{Z}_{L1,L1} & \overline{Z}_{L1,L2} & \overline{Z}_{L1,L3} & \overline{Z}_{L1,PEN} \\ \overline{Z}_{L1,L2} & \overline{Z}_{L2,L2} & \overline{Z}_{L2,L3} & \overline{Z}_{L2,PEN} \\ \overline{Z}_{L1,L3} & \overline{Z}_{L2,L3} & \overline{Z}_{L3,L3} & \overline{Z}_{L3,PEN} \\ \overline{Z}_{L1,PEN} & \overline{Z}_{L2,PEN} & \overline{Z}_{L3,PEN} & \overline{Z}_{PEN,PEN} \end{bmatrix}$$ | $\overline{Z}_{L1,L1} = \overline{Z}_{L2,L2} = \overline{Z}_{L3,L3} = \overline{Z}_{PEN,PEN} =$ $r_v + j0{,}0628\!\left(\ln\dfrac{1}{r'} + 6{,}836\right)$ $\overline{Z}_{L1,L2} = \overline{Z}_{L2,L3} = \overline{Z}_{L3,PEN} = \overline{Z}_{L1,PEN} =$ $j0{,}0628\!\left(\ln\dfrac{1}{D} + 6{,}836\right)$ $\overline{Z}_{L1,L3} = \overline{Z}_{L2,PEN} =$ $j0{,}0628\!\left(\ln\dfrac{1}{D\sqrt{2}} + 6{,}836\right)$ |
| | $$\begin{bmatrix} \overline{Z}_{L1,L1} & \overline{Z}_{L1,L2} & \overline{Z}_{L1,L3} & \overline{Z}_{L1,N} & \overline{Z}_{L1,PE} \\ \overline{Z}_{L1,L2} & \overline{Z}_{L2,L2} & \overline{Z}_{L2,L3} & \overline{Z}_{L2,N} & \overline{Z}_{L2,PE} \\ \overline{Z}_{L1,L3} & \overline{Z}_{L2,L3} & \overline{Z}_{L3,L3} & \overline{Z}_{L3,N} & \overline{Z}_{L3,PE} \\ \overline{Z}_{L1,N} & \overline{Z}_{L2,N} & \overline{Z}_{L3,N} & \overline{Z}_{N,N} & \overline{Z}_{N,PE} \\ \overline{Z}_{L1,PE} & \overline{Z}_{L2,PE} & \overline{Z}_{L3,PE} & \overline{Z}_{N,PE} & \overline{Z}_{PE,PE} \end{bmatrix}$$ | $\overline{Z}_{L1,L1} = \overline{Z}_{L2,L2} = \overline{Z}_{L3,L3} = \overline{Z}_{N,N} =$ $= \overline{Z}_{PE,PE} = r_v + j0{,}0628\!\left(\ln\dfrac{1}{r'} + 6{,}836\right)$ $\overline{Z}_{L1,L2} = \overline{Z}_{L2,L3} = \overline{Z}_{L3,N} = \overline{Z}_{N,PE} =$ $j0{,}0628\!\left(\ln\dfrac{1}{D} + 6{,}836\right)$ $\overline{Z}_{L1,L3} = \overline{Z}_{L2,N} = \overline{Z}_{L3,PE} =$ $j0{,}0628\!\left(\ln\dfrac{1}{2D} + 6{,}836\right)$ $\overline{Z}_{L1,N} = \overline{Z}_{L2,PE} = j0{,}0628\!\left(\ln\dfrac{1}{3D} + 6{,}836\right)$ $\overline{Z}_{L1,PE} = j0{,}0628\!\left(\ln\dfrac{1}{4D} + 6{,}836\right)$ |

## 5

## Harmonic power flow calculation
### Proračun harmoničkih tokova snaga

For the network presented in Fig. 18, several calculations have been performed. The network, as well as harmonic power flow algorithm, have been encoded in Matlab. Harmonic power flows usually converged after 5-6 iterations when the shunt compensation was off. With shunt compensation switched on the iterative process stopped after 120-130 iterations. Demanded calculation precision was 0,001.

The calculations have been conducted in several alternatives:
1) Energy inefficient lighting
2) Energy efficient lighting (CFLs)
3) Induction machines without VSDs
4) Induction machines with VSDs.

At nodes 3 and 5 lighting-type loads were connected (incandescent lamps and CFLs), at node 4 an induction machine was connected (with and without VSD), while at node 6 a linear, resistive-type load was connected at all times.

In Figures 19-23 node voltages are presented. Figures 19 and 20 demonstrate the difference in calculation results for harmonic power flow and simple voltage drop calculation. In these calculations power factor correction capacitors were switched off. The presented curves reveal discrepancies which are due to network's power losses neglecting by the simple voltage drop calculation.

Figures 21-27. show the influence of nonlinear loads on phase voltages, neutral conductor potential and total harmonic distortion throughout the network. The thick lines correspond to simulations when reactive power shunt compensation was switched on and the thinner when shunt compensation was switched off.

Though absolute values of neutral conductor voltages and total harmonic distortion are similar in all cases, it is important to notice that in the case of energy efficient lamps the total lighting power was 80 % less than in the case of
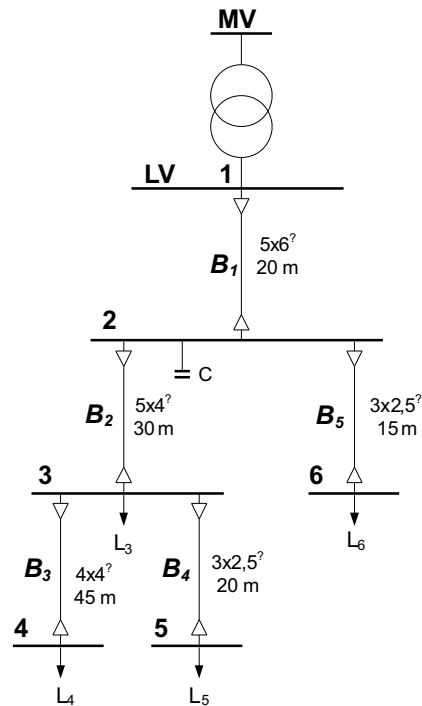
**Figure 18** *Simple low voltage radial distribution network*
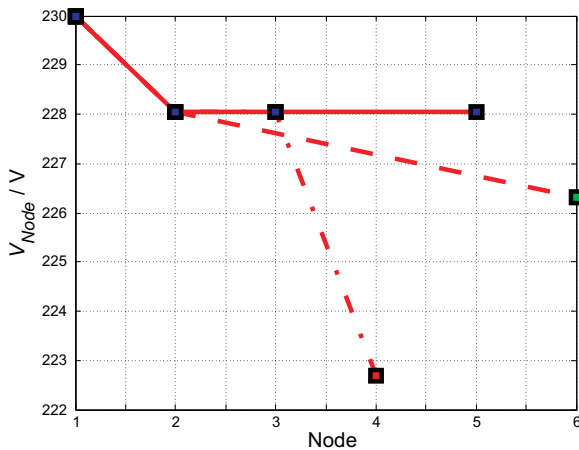**Slika 18.** *Niskonaponska radijalna distribucijska testna mreža*



**Figure 19** *Simple voltage drop calculation - Phase voltages at installation's nodes for a network without nonlinear loads*
**Slika 19.** *Jednostavni proračun pada napona – Efektivna vrijednost faznih napona čvorišta testne mreže u instalaciji bez nelinearnih tereta*
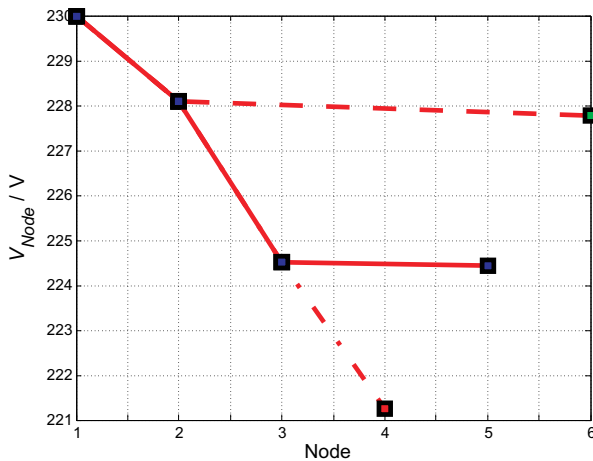


**Figure 20** *Harmonic power flow - Phase voltages at installation's nodes for a network without nonlinear loads*
**Slika 20.** *Harmonički tokovi snaga – Efektivna vrijednost faznih napona čvorišta testne mreže u instalaciji bez nelinearnih tereta*

energy inefficient light sources.

Induction machine operation at partial load with VSD was also investigated, as well as different lighting load-types operation. The results are similar to that presented in the following figures.
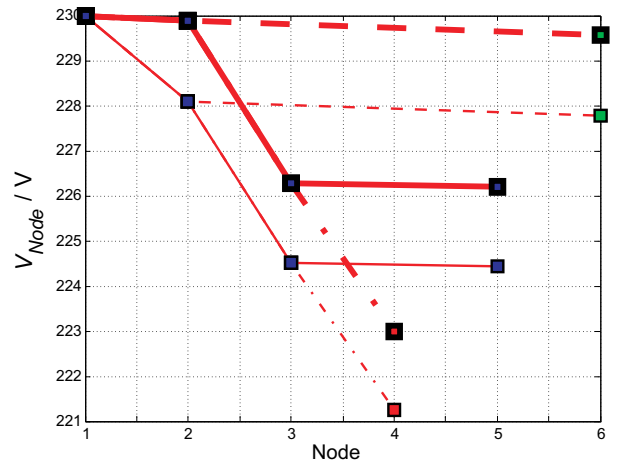


**Figure 21** *Phase voltages at installation's nodes for a network without non-linear loads – energy inefficient lighting*
**Slika 21.** *Efektivna vrijednost faznih napona čvorišta testne mreže u instalaciji bez nelinearnih tereta – neučinkovita rasvjeta*
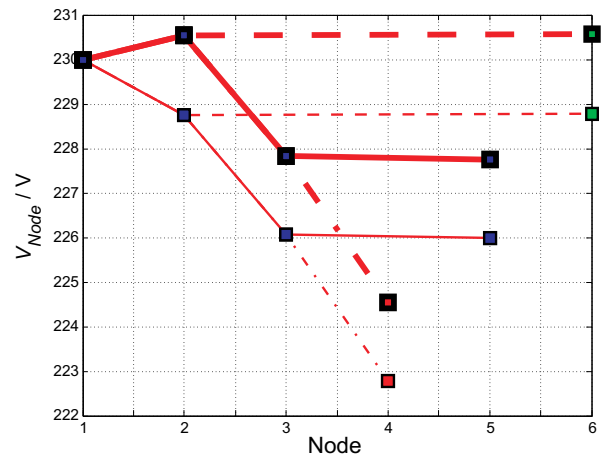


**Figure 22** *Phase voltages at installation's nodes for a network with nonlinear loads - energy efficient lighting*
**Slika 22.** *Efektivna vrijednost faznih napona čvorišta testne mreže u instalaciji s nelinearnim teretima – učinkovita rasvjeta*
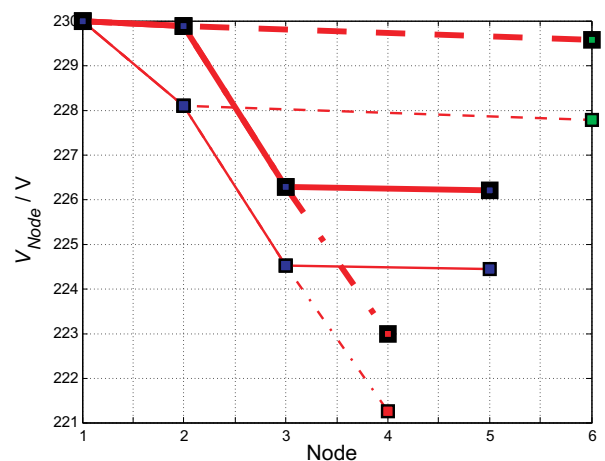


**Figure 23** *Phase voltages at installation's nodes for a network with nonlinear loads – variable speed drive*
**Slika 23.** *Efektivna vrijednost faznih napona čvorišta testne mreže u instalaciji s nelinearnim teretima – frekvencijski pretvarači*
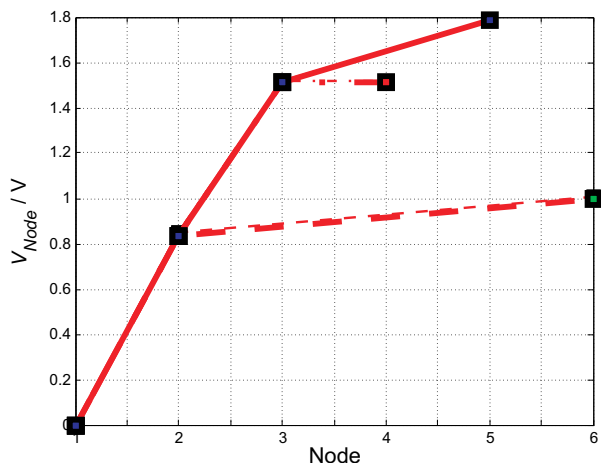
**Figure 24** *Neutral conductor potential at installation's nodes for a network without nonlinear loads*
**Slika 24.** *Efektivna vrijednost napona nulvodiča u čvorištima testne mreže za instalaciju bez nelinearnih tereta*
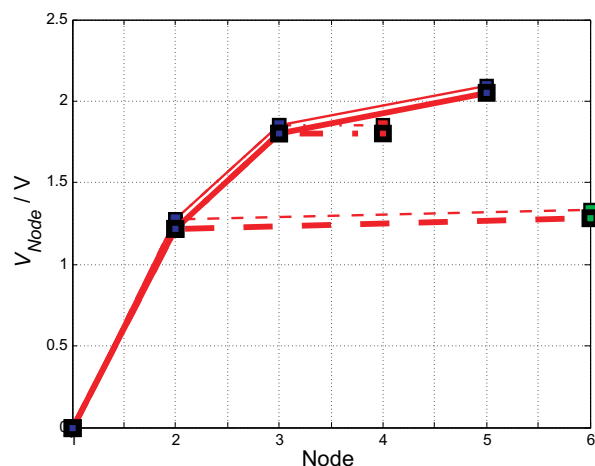


**Figure 25** *Neutral conductor potential at installation's nodes for a network with nonlinear loads*
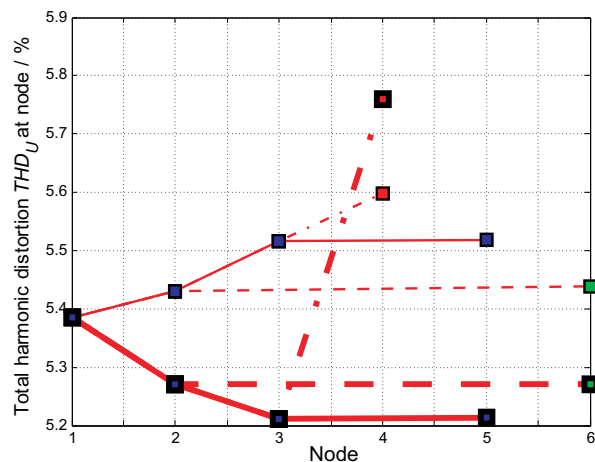**Slika 25.** *Efektivna vrijednost napona nulvodiča u čvorištima testne mreže za instalaciju s nelinearnim teretima*



**Figure 26** *Voltage distortion at installation's nodes for a network with and without nonlinear loads, $THD_U$ at node 1 was 5,39 % in all simulations – capacitive shunt compensation OFF*
**Slika 26.** *Harmoničko izobličenje napona za mrežu s i bez nelinearnih tereta, $THD_U$ u čvorištu 1 iznosio je 5,39 % u svim simulacijama – kompenzacija jalove snage ISKLJUČENA*

Furthermore, in Figures 26 and 27 attenuation of harmonics is observed, due to different load non-linear characteristics and phase connection.

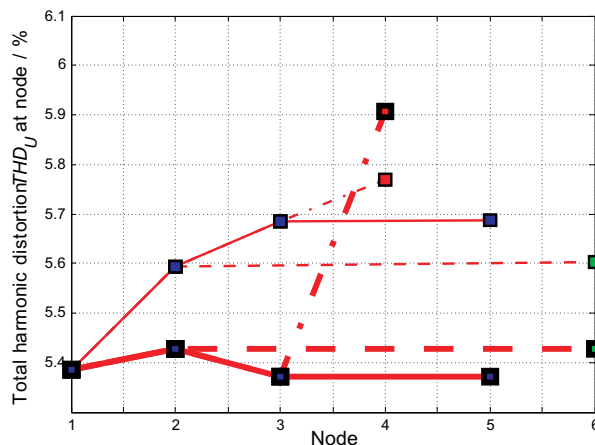In addition, owing to incandescent lamp's inefficiency,



**Figure 27** *Voltage distortion at installation's nodes for a network with and without nonlinear loads, $THD_U$ at node 1 was 5,39 % in all simulations – capacitive shunt compensation ON*
**Slika 27.** *Harmoničko izobličenje napona za mrežu s i bez nelinearnih tereta, $THD_U$ u čvorištu 1 iznosio je 5,39 % u svim simulacijama – kompenzacija jalove snage UKLJUČENA*

power flows and therefore voltage drops are larger than in the same installation, but with energy efficient light sources replacing the inefficient. On the other hand, if energy inefficient light bulbs are replaced with energy efficient ones and VSDs are added to induction machines, fundamental harmonic power flows decrease, while harmonic power flows increase. These harmonic power flows generate unpleasant consequences, described earlier. Especially dangerous can be the effect of neutral conductor overloading which is usually the consequence of considerable 3. harmonic circulation. Afore mentioned is best observed in neutral conductor potential rise in LV installations containing energy efficient lighting. Moreover, harmonics circulation throughout LV installation results in voltage harmonic distortion which in turn can harm sensitive electronic equipment.

After all, it is important to point out the fact, that although individually small, the cumulative impact of all nonlinear loads can considerably overload and distort both low voltage networks and higher voltage networks by harmonics circulation. Fortunately, due to different nonlinear characteristics of such loads, considerable attenuation of harmonics occurs, i.e. cancellation of certain harmonic components, as previously stated. The cumulative impact of all nonlinear loads is, therefore, not equal to their algebraic sum, but rather considerably smaller [20].

# 6
## Conclusion
Zaključak

The intention of this article was to point out the need to take into consideration some other aspects of consistent building's energy efficiency measures implementation which are today, perhaps, underestimated or neglected.

Energy inefficient lighting replacement with energy saving lamps, addition of variable speed drives to existing induction machines, growing presence of efficient electronic equipment in LV installations, by all means, contribute to global electric energy consumption decrease alongside all negative side-effects of electric energy production. However, as previously explained, these electronic devices overload electric networks with harmonic currents and voltages, which under certain circumstances can cause serious problems to other

electronic equipment and network elements themselves.

Nonlinear loads were analyzed, and equivalent models suitable for harmonic power flow presented. Appropriate models of LV cables were developed for inclusion in radial distribution harmonic power flow analysis.

Finally, a simple LV network was modeled and the consequences of one energy efficiency measure implementation were presented. Numerical results were obtained by the simple voltage drop calculation method and harmonic power flow calculation. The influence of reactive power shunt compensation was investigated.

Further research will be focused to harmonic models of other linear and nonlinear network elements and loads, especially efficient lighting (LED) variable speed drives, electronic computers and similar electronic devices. Also, the cumulative impact of such loads on a MV feeder will be investigated.

# 7
# References
Literatura

[1] Pavković, B.; Zanki, V.; Čačić, G. Energetska učinkovitost u sektoru graditeljstva u Hrvatskoj – preliminarne energetske studije. // Strojarstvo, 52, 6(2010).

[2] EN 61000-3-2, Harmonic current emissions, 2005.

[3] Verderver, R. R.; Morse, O. C.; Alling, W. R. Harmonics from compact fluorescent lamps. // IEEE Trans. Ind. Appl. 29, 3(1993), str. 670-674.

[4] Yong, J.; Chen, L.; Nassif, A. B.; Xu, W. A frequency-domain harmonic model for compact fluorescent lamps. // IEEE Trans. on power delivery. 25, 2(2010), str. 1182-1189.

[5] Cunill-Sola, J.; Salichs, M. Study and characterization of waveforms from low-watt (<25W) compact fluorescent lamps with electronic ballasts. // IEEE trans. on power delivery. 22, 4(2007), str. 2305-2311.

[6] Fauri, M. Harmonic modeling of non-linear load by means of crossed frequency admittance matrix. // IEEE Trans. on power delivery. 12, 4(1997), str. 1632-1638.

[7] Cresswell, C.; Djokić, S. Steady state models of low-energy consumption light sources. // 16th PSCC, Glasgow, Scotland, 2008.

[8] Embriz-Santander, E.; Domijan, A.; Williams, C. W. A comprehensive harmonic study of electronic ballasts and their effect on a utility's 12 kV, 10 MVA feeder. // IEEE Trans. on power delivery, 10, 3(1995), str. 1591-1599.

[9] Danfoss. Najvažnije o frekvencijskim pretvaračima. Graphis, Zagreb, 2009.

[10] Eurovent certification company. URL: http://www.eurovent-certification.com (13.10.2010.)

[11] Kathöfer, T. Zur Leistungsanpassung durch Drehzahl-regelung bei Kompressions – Kälteanlagen mit Hubkolben-verdichter und Drehstrom – Antriebsmotor. // Dissertation, Technisches Universität Berlin, 1990.

[12] Task force on harmonics modeling and simulation, IEEE PES Harmonic working group, IEEE Trans. on power delivery, 16, 4(2001), str. 791-800.

[13] Saniter, C., Wood, A., R., Hanitsch, R., Schulz, D., Modeling the effects of AC system impedance unbalance on PWM converters using frequency coupling matrices, Power Tech conference proceeding, Bologna, 2 (2003)

[14] Square D. Power system harmonics-Causes and effects of variable frequency drives. // Bulletin No. 8803PD9402, Raleigh, USA, August, 1994.

[15] Ahmadi, G.; Shahrtash, S. M. Neutral to earth voltage analysis in harmonic polluted distribution networks with multigrounded neutrals. // World academy of science, engineering and technology, 49(2009), str. 905-909.

[16] Teng, J., Chang, C. Backward/forward sweep-based harmonic analysis method for distribution systems. // IEEE Trans. on power delivery, 22, 3(2007), str. 1665-1672.

[17] Teng, J.; Chang, C. A fast harmonic load flow for industrial distribution systems. // Powercon, Perth, Australia, 2000. str. 1149-1154.

[18] Teo, C., Y.; He, B., G. Integrating three-phase load flow and short-circuit current calculation for a low voltage system. // Electric power systems research, 53, (2000), str. 123-132.

[19] Li, F.; Broadwater, R.; Sargent, A. Cable impedance calculations with parallel circuits and multi-neutral returns in distribution networks. // Journal of Marine Science and Technology. 18, 2(2010), str. 290-297.

[20] Mansor, A.; Grady, W. M.; Chowdhury, A. H.; Samotyj, M. J. An investigation of harmonics and diversity among distributed single-phase power electronic loads. // IEEE Trans. on power delivery. 10, 1(1995), str. 467-473.

**Author's addresses**
Adrese autora

***Dr. sc. Dubravko Franković, dipl. ing. el.***
Sveučilište u Rijeci
Tehnički fakultet
Zavod za elektroenergetiku
Vukovarska 58
51000 Rijeka, Croatia
Email: dubravko.frankovic@riteh.hr

***Red. prof. dr. sc. Branimir Pavković, dipl. ing. stroj.***
Sveučilište u Rijeci
Tehnički fakultet
Zavod za termodinamiku i energetiku,
Vukovarska 58
51000 Rijeka, Croatia
Email: branimir.pavkovic@riteh.hr

***Mr. sc. Matko Bupić, dipl. ing. stroj.***
Sveučilište u Dubrovniku
Pomorski odjel
Ćira Carića 4
20000 Dubrovnik, Croatia
Email: matko.bupic@unidu.hr